










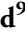

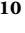

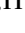



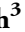



Stalk cell polar ion transport provide for bladder-based salinity tolerance in *Chenopodium quinoa*

Nadia Bazihizina^{1,2*} , Jennifer Böhm^{3*} , Maxim Messerer^{4*} , Christian Stigloher⁵ , Heike M. Müller³ , Tracey Ann Cuin⁶ , Tobias Maierhofer³ , Joan Cabot⁷ , Klaus F. X. Mayer⁴ , Christian Fella⁸ , Shouguang Huang³ , Khaled A. S. Al-Rasheid⁹ , Saleh Alquraishi⁹ , Michael Breadmore¹⁰ , Stefano Mancuso¹ , Sergey Shabala^{2,11} , Peter Ache³ , Heng Zhang¹² , Jian-Kang Zhu^{12,13} , Rainer Hedrich³  and Sönke Scherzer³ 

¹Department of Agriculture, Food, Environment and Forestry (DAGRI), University of Florence, Viale delle Idee 30, 50019 Florence, Italy; ²College of Science and Engineering, Tasmanian Institute for Agriculture, University of Tasmania, Private Bag 54, Hobart, Tas. 7001, Australia; ³Institute for Molecular Plant Physiology and Biophysics, University of Wuerzburg, Julius-von-Sachs Platz 2, 97082 Wuerzburg, Germany; ⁴Plant Genome and Systems Biology, Helmholtz Center Munich, Ingolstädter Landstraße 1, 85764 Neuherberg, Germany; ⁵Imaging Core Facility, Biocenter, University of Wuerzburg, Am Hubland, 97074 Wuerzburg, Germany; ⁶Biological Sciences, School of Natural Sciences, University of Tasmania, Private Bag 55, Hobart, Tas. 7001, Australia; ⁷Diagnostic Devices Unit, LEITAT Technological Center, Innovació 2, Terrassa 0822, Barcelona, Spain; ⁸Fraunhofer IIS, Nano CT Systeme, Josef-Martin-Weg 63, 97074 Wuerzburg, Germany; ⁹Zoology Department, College of Science, King Saud University, PO Box 2455, Riyadh 11451, Saudi Arabia; ¹⁰School of Natural Sciences, Australian Centre for Research on Separation Sciences (ACROSS), University of Tasmania, Private Bag 75, Hobart, Tas. 7001, Australia; ¹¹International Research Centre for Membrane Biology, Foshan University, Foshan 528000, China; ¹²State Key Laboratory of Plant Molecular Genetics, Shanghai Center for Plant Stress Biology, CAS Center for Excellence in Molecular Plant Sciences, Chinese Academy of Sciences, Shanghai 200032, China; ¹³Institute of Advanced Biotechnology and School of Life Sciences, Southern University of Science and Technology, No. 1088, Xueyuan Avenue, Shenzhen, Nanshan District, China

Summary

Authors for correspondence:

Sönke Scherzer

Email: soenke.scherzer@uni-wuerzburg.de

Rainer Hedrich

Email: hedrich@botanik.uni-wuerzburg.de

Christian Stigloher

Email: christian.stigloher@uni-wuerzburg.de

Received: 18 November 2021

Accepted: 12 April 2022

New Phytologist (2022) **235**: 1822–1835

doi: 10.1111/nph.18205

Key words: halophyte, polar ion transport, quinoa, salt tolerance, stalk cell.

- *Chenopodium quinoa* uses epidermal bladder cells (EBCs) to sequester excess salt. Each EBC complex consists of a leaf epidermal cell, a stalk cell, and the bladder.
- Under salt stress, sodium (Na⁺), chloride (Cl⁻), potassium (K⁺) and various metabolites are shuttled from the leaf lamina to the bladders. Stalk cells operate as both a selectivity filter and a flux controller.
- In line with the nature of a transfer cell, advanced transmission electron tomography, electrophysiology, and fluorescent tracer flux studies revealed the stalk cell's polar organization and bladder-directed solute flow.
- RNA sequencing and cluster analysis revealed the gene expression profiles of the stalk cells. Among the stalk cell enriched genes, ion channels and carriers as well as sugar transporters were most pronounced. Based on their electrophysiological fingerprint and thermodynamic considerations, a model for stalk cell transcellular transport was derived.

Introduction

Sodium (Na) toxicity is the main physiological constraint that affects crop performance under long-term salinity exposure (Zörb *et al.*, 2019). Halophytes take up Na⁺ and chloride (Cl⁻) ions and sequester the toxic load to specialised dumping sites within the plant. Approximately 50% of all halophyte species do this by loading salt into extra-epidermal structures called salt bladders

(or epidermal bladder cells; EBCs). Epidermal bladder cells are arguably the most remarkable anatomical feature of halophytes, allowing them to sequester excessive Na⁺ away from metabolically active cells of the vulnerable growing plant (Flowers & Colmer, 2008). With a diameter as much as ten times that of epidermal cells (ECs), each EBC is able to sequester 1000 times more Na⁺ than an EC (Shabala *et al.*, 2014). Being so large (up to 200 µm in diameter), quinoa EBCs represent an ideal model with which to study the mechanisms of ion sequestration. Importantly, and contrary to existing plant model systems in salinity

*These authors contributed equally to this work.

tolerance research, quinoa is widely used as a pseudo-cereal crop and is of high economic importance. Furthermore, being a true halophyte, quinoa plants actually benefit from having high concentrations of sodium in the growth media (Koyro & Eisa, 2008; Hariadi *et al.*, 2011).

In 2017, the genome of quinoa was made publicly available (Yasui *et al.*, 2016; Jarvis *et al.*, 2017; Zou *et al.*, 2017) and from bioinformatic analysis of the RNA profile, we gained access to the molecular code of the salt bladder complex (Zou *et al.*, 2017; Bohm *et al.*, 2018). Electrophysiological studies revealed that loading of Na^+ and Cl^- into EBCs is mediated by a set of tailored plasma and vacuole membrane-based sodium-selective channels and Cl^- -permeable transporters (Bohm *et al.*, 2018). Uphill transport and accumulation of Na^+ and Cl^- is indirectly energised by plasma- and tonoplast-based H^+ pumps, while sugar and solute transporters enable the unidirectional movement of high-energy saccharides and compatible osmolytes from the mesophyll via the epidermis and stalk cell into the EBCs.

In contrast to EBCs, nothing is known about the molecular nature and a role of the stalk (SCs) cells in this process. Stalk cells connect, and act as a transfer cell between, the ECs and the EBCs, thus assuming the critical function of 'traffic controller'. Consequently, in the present study we asked how SCs mediate transcellular Na^+ , Cl^- and K^+ fluxes alongside those of sugars and metabolites, to supply solutes and water for growth and expansion of the bladder and for the EBCs to function as major salt storage sites.

Materials and Methods

Quinoa plants (*Chenopodium quinoa* Willd.) were grown from seeds in 15 cm diameter pots filled with standard potting mix under temperature-controlled glasshouse conditions. The plants were grown under a 16 h : 8 h, 20°C : 15.5°C, day : night photoperiod (incandescent lights were set at 06:00 h to 09:00 h and 16:00 h to 22:00 h to give a consistent day length) with a mean humidity of 74%. Plants were either watered with tap water (control) or with 100–300 mM NaCl for the entire duration of the experiment.

Stalk cell isolation and net ion flux and membrane potential measurements

Stalk cells were isolated from detached leaves or small sections of the petioles taken from 5-wk-old plants. In petioles the SCs were isolated by immobilising the petioles in a measuring chamber containing 4 ml basal salt medium (BSM: 0.5 mM KCl, 0.1 mM CaCl_2 , pH 5.5) 1 h before to measurement. The petioles were then lightly brushed with a fine paintbrush (diameter 2 mm) to remove the EBCs and the BSM was changed twice to remove all detached bladders. These isolated SCs were then used for *in vivo* ion flux and membrane potential measurements using the microelectrode ion flux estimation (MIFE, University of Tasmania, Hobart, Tas., Australia) or scanning ion selective electrodes (SISE) as described by

Shabala *et al.* (2006) and Scherzer *et al.* (2017), respectively. Details on the fabrication and calibration of the microelectrodes and the measurements are available in the Supporting Information Methods S1.

Stalk cells were also isolated from the leaves. The detached leaves were submerged in BSM and lightly brushed, as for the petioles, to remove EBCs. Since the bladder cells are very hydrophobic, the success of the brushing is easy to monitor. The abaxial epidermis containing the SCs was then removed using fine tweezers for staining with fluorescein diacetate (FDA) or for RNA sequencing (RNA-seq). As an SC-free negative control, leaves still attached to the plants were forcefully brushed (i.e. hard brushing) with the epidermal peels collected 30 min later (to ensure that any viable stalk cells would dry). Intact segments of nonbrushed leaves were used as positive controls.

To validate our approach, we did the following: performed a principal component analysis (PCA, Fig. S1a); compared the DEGs obtained here from EBCs with those obtained from isolated EBCs (Bohm *et al.*, 2018); compared the expression of trichome-specific genes (Jakoby *et al.*, 2008) between the different samples (Fig. S2a); and analysed the function of genes whose expression increased > 10-fold in the lightly-brushed samples, relative to the hard-brushed samples. All these results verified that the brushing approach is an appropriate method for the analysis of different cell types (Methods S1).

RNA sequencing

For RNA-seq, only nonsalinised plants were used and, after removing the abaxial epidermis, the peel was quickly placed in RNAlater Stabilization Solution (Thermo Fisher Scientific, Wilmington, DE, USA) and then processed. Total RNA was isolated using the NucleoSpin RNA Plant Kit (Macherey-Nagel, Düren, Germany) and RNA was eluted in 33 μl RNase free water. Quality control measurements were performed on an Experion™ automated electrophoresis station (Bio-Rad) and the concentration was determined using a Nanodrop ND-1000 spectrophotometer (Thermo Fisher Scientific). Detailed descriptions of the RNA-seq library preparation and sequencing and the processing of raw RNA-seq data, mapping and differential gene expression (DGE) analysis are provided in Methods S1.

Xenopus oocyte recordings

To investigate the nature of the transporters giving rise to the SC polar ion transport detected by the *in vivo* MIFE experiments shown in Figs 3, 4, and S9, we screened the RNA-seq data. Inspection of the RNA-seq data set revealed the coding sequences (CDS) for the following ion transport proteins: CqSKOR (TRINITY_GG_83_c4_g1), CqSLAH3 (TRINITY_GG_29628_c18_g1), and CqAMT1 (TRINITY_GG_1769_c6_g1). To investigate their transport activity via heterologous expression in *Xenopus* oocytes, cDNAs of the transport proteins were generated and analysed using *Xenopus* oocytes. Details about cDNA and cRNA preparation, oocyte preparation and cRNA injection are described in Methods S1.

Ion flux and membrane potential measurements

For ion flux measurements the MIFE (University of Tasmania, Hobart, Tas., Australia) technique and the SISE (Scanning Ion Selective Electrodes) technique was applied. Details regarding flux estimations are described in Methods S1.

Images of stalk and bladder cell density

Images of the EBCs from the abaxial leaf samples were obtained using an environmental scanning electron microscope (FEI MLA650 ESEM; Thermo Fisher Scientific). Abaxial leaf samples, without any treatment, were examined at 25 kV and 600 Pa, with a *c.* 10 mm working distance at *c.* 5.0°C. Images of the leaves and SCs were obtained using a conventional digital camera. Further details regarding image generation are provided in the Methods S1. All images were processed using IMAGEJ (v.1.51).

Esculin uptake

For the esculin uptake measurements, two different experimental set-ups were used. For the first set-up, quinoa leaves with petioles were detached from plants grown under control conditions. The petiole was placed in the 1 mM esculin (Merck, Darmstadt, Germany)-containing BSM solution for 1 h. For the second set-up, epidermal peels were fixed to a pipette tip and incubated for 1 h in 1 mM esculin-containing BSM solution. The measurements were performed on a SP5 confocal laser scanning microscope (Leica Microsystems CMS GmbH, Mannheim, Germany) using a water immersion objective lens (HCX IRAPO L ×25/0.95 W; Leica) for confocal imaging. Esculin was excited with a 405 nm diode laser, and emission was detected between 409 and 479 nm. Chlorophyll auto-fluorescence was detected between 630 and 738 nm.

Capillary electrophoresis

The sap content of bladder cells was collected from quinoa leaves of plants grown under control or salt stress (100 mM and 300 mM NaCl) using sharp glass capillaries impaled into bladder cells. Details regarding the sample preparation, reagents and procedures used are provided in Methods S1.

Results

What structure enables stalk cells to become transfer cells?

In this study we focused on the function of SCs, which connect the photosynthetically active leaf tissue to the EBCs (Fig. 1a). To characterise the specific ultrastructure of quinoa SCs, we peeled epidermal strips from the abaxial and adaxial sides of leaves and processed them for high-pressure freezing and freeze substitution. To readily identify and precisely locate SCs for the preparation of ultrathin sections, resin blocks were first scanned in a nanoCT-setup for X-ray assisted identification of target cells for three-dimensional electron microscopy (3D-EM) (Karreman *et al.*,

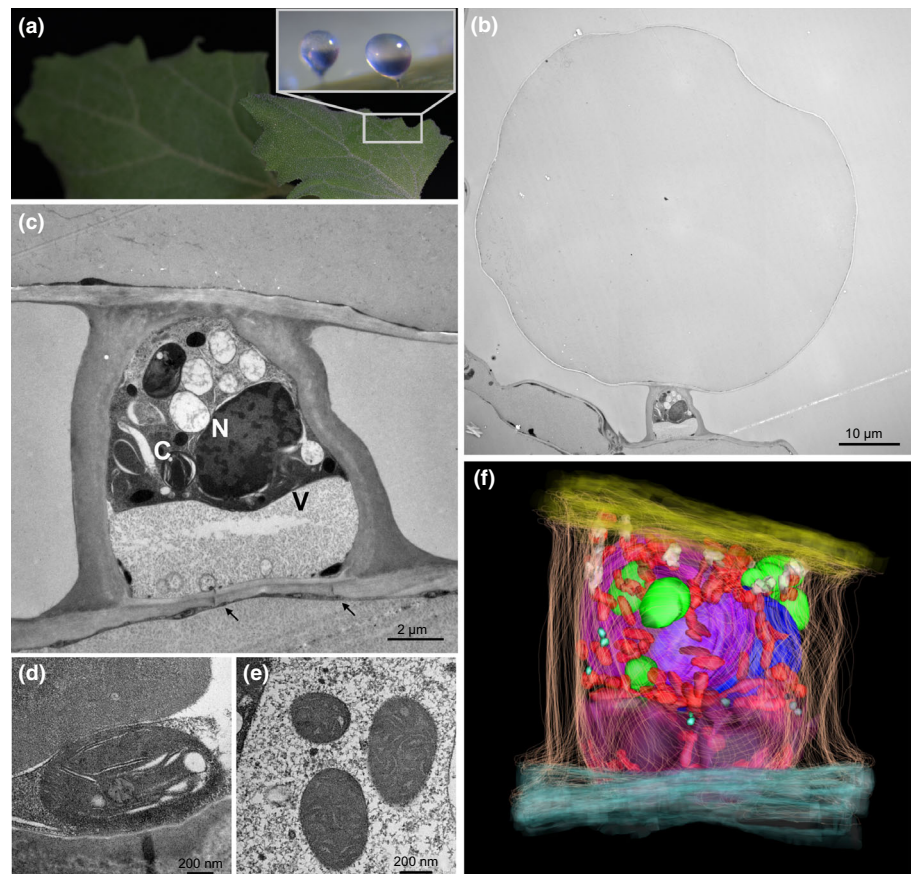
2017). The resulting tomogram stack was then used as a 3D map to readily target the identified SC in the ultracut setup (Video S1) for subsequent analyses using transmission electron microscopy (TEM; Kremer *et al.*, 1996).

The electron micrographs and the resulting 3D reconstruction (Figs 1b–f, S3a–e) of SCs revealed an ultrastructure that contains a large nucleus, chloroplasts, endoplasmic reticulum, and multi-vesicular bodies (Fig. S3a,b). Oleosomes and plastid-like organelles can also be seen (Fig. 1c,d). Harbouring most of the organelles, the cytoplasm appears densely packed. Numerous mitochondria are found embedded in this dense cytoplasm, indicating a large respiratory capacity, and the high number of mitochondria in the apical part of the SC implies high rates of energy consumption (Figs 1c,e, S3c). This zone, which faces the EBC, would be expected to have high solute transport activity. Interestingly, just at the apical side, Golgi complexes could be found (Fig. S3a). The relatively high amount of euchromatin in the large nucleus also suggests that SCs are highly metabolically active (Fig. 1c). The cell wall at the lateral sides of the stalk is thicker and appears more electron dense than at the sides neighbouring the bladder and epidermis (Figs 1c, S3d). We were able to correlate this observation with the RNA-seq data, which were enriched for ‘cell wall proteins’. The basal and the apical cell wall were found to be decorated by plasmodesmata (PD)-like structures (Figs 1c, S3f). When the PD were open, ions and small sized metabolites could enter the SC via the adjacent epidermis cell by diffusion though these plasma bridges and/or plasma membrane transporters. Plasmodesmata are filled with electron dense material that might reduce the free diffusion of bulky solutes. In spite of this, vesicular structures in the stalk cells appear often in close contact to the PDs (Fig. 1c). This scenario has been associated with active transport across the electron dense PD structures via exocytosis/endocytosis (Cilia & Jackson, 2004). Epidermal bladder cells develop an extra-large central storage vacuole, but in SCs fragmented vacuoles are often present (Fig. S3e) (Reisen *et al.*, 2005), and these are not expected to play a dominant role in SC transcellular transport. In addition, the presence of multi-vesicular bodies points to a high degree of recycling activity of the membrane proteins in SCs (Fig. S3b).

The transcriptome mirrors the structure and function of a transfer cell

We recently performed transcriptional analysis of quinoa using RNA-seq to gain insights into the expression profiles of mechanically-isolated EBCs (Bohm *et al.*, 2018). To achieve a similar understanding of the molecular biology of SCs alone and carry out similar procedures on SCs, we submerged detached leaves in buffer, then lightly brushed the abaxial surface with a fine paintbrush to gently remove the EBCs. The abaxial epidermis was then removed using tweezers and sampled in buffer for RNA extraction and RNA sequencing. This way we obtained three epidermal cell populations: nonbrushed samples with intact EBCs and SCs, lightly brushed samples with the EBCs removed by retained SCs, and hard-brushed samples with SCs and EBCs destroyed (Fig. S4a). Viability staining showed in all three

Fig. 1 Ultrastructure of near-to-native preserved epidermal preparations, revealing distinct characteristics of stalk cells. (a) A leaf of *Chenopodium quinoa* grown under control conditions. The inset image shows epidermal bladder cells (EBCs) with stalk cells (SCs) on the leaf surface. (b) Low magnification transmission electron micrograph of an EBC and corresponding SC (magnified in (c)). (c) Transmission electron micrograph of SC at a higher magnification. The nucleus (N), vacuole (V) and one chloroplast (C) are indicated. The large amount of euchromatin in the large nucleus (open chromatin) is visible as lighter grey tones in the chromatin structure. In addition, two plasmodesmata are visible in the basal cell wall (arrows). (d, e) More highly magnified details of SC cellular ultrastructure from different sections ((d) chloroplast, (e) mitochondria). (f) Three-dimensional reconstruction of the SC ultrastructure: basal (epidermal) cell wall (blue), apical (bladder-facing) cell wall (yellow), lateral (outer) cell wall illustrated in fine lines, chloroplast (green), nucleus (dark blue), fragmented vacuoles (purple), mitochondria (red), Golgi complexes (grey), multivesicular-bodies (turquoise). (See also Supporting Information Fig. S3; Video S1). Bars: (b) 10 μ m; (c) 2 μ m; (d, e) 200 nm.



epidermis collections living GCs and only dead common ECs (Fig. S4d–g). In lightly brushed samples (Fig. S4d–f) the bladder was removed and the living SCs were preserved. As a negative SC-free control, leaves were forcefully brushed to destroy SCs and EBCs (Fig. S4g). These samples were sequenced to evaluate SC-specific expression profiles and to identify differentially expressed genes (DEGs) in the SC-enriched and EBC-enriched fractions (Figs S1a, S4a).

After filtering for weakly expressed transcripts, we found that 79 883 of 113 451 transcripts (70.4%) were expressed in all three RNA-seq samples (nonbrushed, lightly brushed, and hard-brushed). Sample differential analysis detected 5109 DEGs (4612 with high confidence) for SCs and 1591 (1431 with high confidence) for EBCs (false discovery rate (FDR) < 0.05) (Table S1a–c). The EBC complex evolved from typical trichomes (Shabala *et al.*, 2014). Thus, to confirm whether our approach enabled the isolation of SCs and the detection of cell type-specific genes, we used trichome-specific genes as SC–EBC marker genes. Using a published dataset of highly trichome-specific genes in *Arabidopsis* (Jakoby *et al.*, 2008), we identified their orthologs in our data and compared their expression of the three samples (nonbrushed, lightly brushed and hard-brushed) (Fig. S2a). A significantly higher expression of the trichome-specific genes was found in the lightly brushed and nonbrushed samples compared to the hard-brushed sample, confirming the high cell purity of the samples.

The high number of SC-related DEGs suggests that these cells have more altered gene expression compared to EBCs (Fig. S2). That > 80% of DEGs in EBCs are downregulated implies that these large cells require fewer genes to drive solute deposition than the SCs, which serve as transfer cells to supply EBCs with ions and metabolites.

To compare SC with EBC gene expression, we annotated our dataset with MAPMAN BINs (Thimm *et al.*, 2004) and a metabolic pathway description to allow filtering by genes according to their function and metabolic activity. On a global view, in all 29 major MAPMAN BINs, a higher number of DEGs were found in SCs compared to EBCs (Table S1a–c; Fig. S2b).

In line with the TEM-based nuclear structure, we found over 10-fold more DEGs in SCs related to chromatin reorganisation than in the EBCs. In this context, it is worth mentioning that chromatin reorganisation has previously been associated with salinity stress (Kim *et al.*, 2015; Probst & Mittelsten, 2015). Although leaf abscisic acid (ABA) concentrations increase under salt stress (Ruiz-Sola *et al.*, 2014), individual BINs for ABA synthesis, import and signalling were found to be largely underrepresented in SCs (Table S1d,e), indicating that a salt stress response via ABA-signalling does not play a major role in SCs.

In the MAPMAN metabolic pathway description we spotted five differentially expressed PD-related genes (four up, one down, Table S1s). Among them were PDLPs (plasmodesmata-located proteins), which have already been shown to regulate the

intercellular permeability of PDs (Ye *et al.*, 2017; Liu *et al.*, 2020). At a high pressure (turgor) difference between neighbouring cells – and very likely other stress or developmental conditions too – PDs can close completely (Park *et al.*, 2019), and under such circumstances Ca^{2+} may have a regulatory function as well (Tucker, 1990).

Epidermal bladder cells have only a few chloroplasts without grana (Bohm *et al.*, 2018), whereas SCs contain fully developed chloroplasts. However, of the 749 MAPMAN annotated photosynthesis genes, only a few are differentially expressed in SCs (22) and EBCs (six). By contrast, of the 1826 MAPMAN annotated chloroplast related genes in SCs and EBCs, only 84 and 18 (respectively) were differentially regulated, implying that photosynthesis in SCs is solely used for light sensing and/or direct energy production by the supply of reduction equivalents (Table S1f,g).

Because SCs contain a high number of oleosomes and a thick cuticle, we analysed the 1210 genes associated with ‘lipid metabolism’ (MAPMAN BIN 5) (Table S1h). Among them, 114 were significantly differentially expressed in SCs (28 higher) and 44 in EBCs (12 higher). Genes involved in ‘fatty acid synthesis’ were the most numerous in both SCs (24.6%) and EBCs (31.8%). The analysis of enriched Kyoto Encyclopedia of Genes and Genomes (KEGG) identifiers showed pathways significantly upregulated for fatty acid elongation and linoleic acid metabolism (Fig. S1b).

How is the transfer cell polarised?

Stalk cells grow a thick cell wall at the epidermal-facing side. In line with the SC’s ultrastructure, we found 1183 genes annotated for ‘cell wall’ (MAPMAN BIN 21). The highest upregulated DEGs were ‘cell wall proteins’ (upregulated 681-fold) and the most numerous DEGs were found for ‘pectin’ (30.3%), ‘hemicellulose’ (15.0%) and ‘cutin and suberin’ (15.0%) (Fig. S2b).

Because of the bipolar SC anatomy, we searched our database for polarity-related genes. Root hairs are also polar-growing cells, and interestingly we found the highest expression of root hair-related genes in SCs, with far less in EBCs. For outer, inner, and planar polarity, TWD1, D6PK, ROP, ACT7 and AP2 are involved in Arabidopsis roots (Yang, 2008; Nakamura & Grebe, 2018). All of these genes showed higher expression in SC, except for the transcription factor AP2. We also found no ROP genes, but did find ROP binding protein kinases, ROP guanine nucleotide exchange factors, ROP interactive partners and ROP-interactive CRIB motif-containing proteins (Fig. S2b).

Given that SCs only have a few small vacuoles, we filtered for genes associated with the vacuolar membrane (VM) and plasma membrane (PM). We searched our data for gene ontology (GO) terms GO: 0005774 (VM) and GO: 0005886 (PM) and found 114 and 1166, respectively. For VM we found eight DEGs (two up, six down) and for PM, 149 DEGs (39 up, 110 down). Plasma membrane-related genes were higher in SCs than in EBCs and the bulk of the leaf. It is also worth mentioning that aquaporins, including

four PIP1s (4.8, 5.1, 9.1 and 359-fold) and four NIPs (4.1, 5.9, 6.3 and 7.8-fold) were exclusively found to be induced in SCs (Table S1i; Fig. S2b). To investigate for symplastic conductivity, we made use of membrane-impermeable but PD permeable dyes. After loading of Lucifer yellow (LY) through the petiole or active ionophoretic loading via intracellular microelectrodes inserted into epidermal cells, LY fluorescence propagated and stained SCs but not the adjacent EBCs (Fig. S5a,b). This indicates that an open symplastic junction exists between the basal EC of the SC but not between the SC and the EBC. To test this assumption, we loaded via an external pipette the EBC apical pole with 5-(and-6)-carboxyfluorescein diacetate (CFDA). In the bladder pole CFDA is split by decarboxylases into FDA. As a result, FDA fluorescence was initiated immediately after loading and propagated throughout the entire EBC. However, even after 4 h – a time at which the bladder was FDA glowing – no staining of the SC was observed (Fig. S5c). Together these results show that at the given developmental state of the EC–SC–EBC complex, the symplastic junctions between ECs and SCs are open, but those between SCs and EBCs are closed. Together these findings support the notion that SCs operate as flux controllers for bladder-directed trafficking of water and solutes.

Finally, we wanted to elucidate the molecular mechanisms underlying the ability of SCs to transport high loads of salt from leaves to the EBCs. Taking a closer look at the transporters of these cells (Table S1j–o), we found that the most abundant differentially regulated pathways in both cell types were associated with solute transport. This suggests that the regulation and turnover of osmolyte transport proteins is pronounced in SCs, providing EBCs with vital salt deposit functions via transcellular solute flow. The enrichment of MAPMAN BINs, GO terms and KEGG pathways showed more over- and under-representation in SCs compared to EBCs (Figs S1b, S6–S8). To gain insight into the nature of transporters expressed by the transfer cell, we filtered our DEG list for MAPMAN annotation ‘solute transport’ (MAPMAN BIN 24), finding 3886 annotated genes, 362 DEGs (157 up, 205 down, Table S1j; Fig. S2b) in SCs. Significantly, the most upregulated was ‘primary active transport’.

Analogous to the SCs feeding the EBCs, phloem companion cells (CCs) nurse the sieve tube. We compared our data with different published CC-specific datasets: an Arabidopsis phloem CC-specific transcriptome (Table S1q) (You *et al.*, 2019), a collection of CC-ESTs (Table S1r) (Deeken *et al.*, 2008) and ion channel function in CCs (Ivashikina *et al.*, 2003; Deeken *et al.*, 2008). This comparison points towards increased CC-comparable gene expression in SCs compared to EBCs and strongly supports the hypothesis of a transfer cell function for the SCs (Fig. S2b).

Energetics of the transcellular transport in stalk cells

The movement of salts and metabolites across the SC can be mechanistically compared to that associated with epithelial transport (e.g. desalting by the kidney). The basic feature of kidney

epithelial cells is a membrane potential difference between the basal and apical side (Pu *et al.*, 2015). This electrical gradient, together with the polar organisation of ion transporters, enables Na^+ and Cl^- uptake at the basal side with release at the apical side. The SC is sandwiched between a large common EC at its basal pole and the giant EBC on the apical end (Figs 1, 2). To experimentally confirm the trans-SC voltage gradient experimentally, we stained intact SCs with the voltage-sensitive fluorescent dye ANNINE-6plus (Sensitive Farbstoffe, Munich, Germany). The different fluorescence intensities of the SC PM are in line with a hyperpolarised membrane potential at the pole facing the epidermis relative to the bladder directed one (Fig. S5d). Under the light microscope the SC appears as a weakly structured cell type, dominated by a large nucleus (Figs 2, S5d) and covered laterally by a thick cell wall and cuticle (Figs 1c,f, S3d), which likely prevents ion leakage to the extracellular medium and electrically isolates the SC. Unfortunately, this isolation prevents monitoring of ion transport within the transfer cells via voltage recording microelectrodes (Scherzer *et al.*, 2017; Dindas *et al.*, 2018).

To overcome this problem, we gently brushed quinoa leaves to remove the bladders. This maintained the vitality and transport activity of the transfer cell as demonstrated by the vitality staining and membrane potential recordings, respectively (Figs 3a, S4b–g). Petioles with the stalk's apical surface exposed were polarity immobilised in a measuring chamber, and the membrane was hyperpolarised to -116 mV. When plants were grown in the presence of 200 mM NaCl for 5 wk, the membrane potential dropped by 29 mV (Fig. 3a). Pre-treatment with 0.5 mM sodium orthovanadate for 1 h further increased the extent of membrane depolarisation, with potentials under control and saline conditions declining to -65 and -61 mV, respectively. This indicates that the membrane potential, and very likely SC transport, is ATP energy dependent. In sub-BIN 24.1 'primary active transport' we find P-type ATPases; 12 of them are differentially expressed in SC-enriched fractions (three up, nine down) and only four (all down) in EBC-enriched fractions. Among the ABC transporters ('ABC superfamily', MAPMAN BIN 24.1.3), we found 13 upregulated genes (ABCB1, ABCC10, ABCG3 and ABCG37) with a highest fold-change of 171 (ABCG37), while for EBCs, only two were upregulated ($2\times$ ABCG31) (Table S1a).

Stalk cells shuttle ions and sugar towards the salt bladder

Stalk cells (Figs 1, 2) and EBCs have only a few chloroplasts. Thus, to maintain energy metabolism, sugars need to be imported from mesophyll cells, the main producers of saccharides. Consequently, the SCs must operate systems that allow sugar intake from the EC, with its further release into the EBC. Like other plant sugar transport systems such as the phloem, sucrose could enter the SC via a H^+ -driven sugar importer of the SUC-type, while its release could be mediated by a SWEET-type facilitator. It is of note that transcripts for both sugar transporter types were found in SCs (Table S1o; Fig. S2b). Besides sucrose, esculin is a substrate for dicot SUT- and SWEET-type transporters. Type I sucrose transporters such as SUC2 and SUC9 from *Arabidopsis* conduct esculin at an equal rate to that of

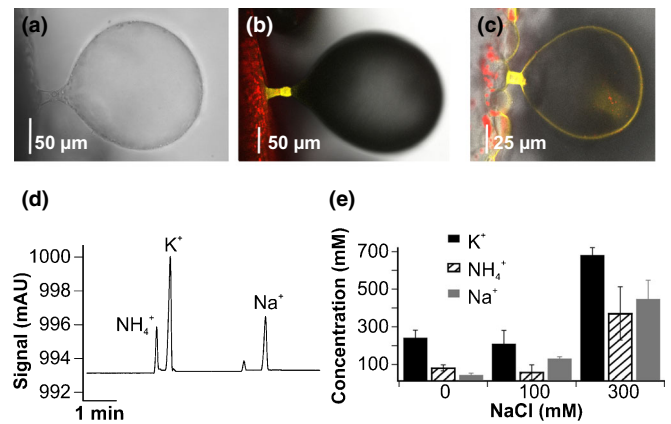


Fig. 2 Sugar and cation sequestration in bladder cells. (a) Light microscopic image of a *Chenopodium quinoa* epidermal–stalk–bladder cell complex. (b, c) Using the fluorescent β -glucoside esculin, transcellular sugar transport through stalk cells could be seen (b). The sucrose substitute travelled along the epidermal cell, though the stalk cell and ended up in the bladder cytoplasm (c). Representative images are shown. (d) Electropherograms of bladder sap collected from fully expanded leaves of quinoa plants grown with different NaCl concentrations (0, 100, 300 mM NaCl) and analysed using the capillary electrophoresis (CE) technique revealed the cations ammonium (NH_4^+), sodium (Na^+), and potassium (K^+). (e) Statistical analysis of the cation concentration in bladder cells determined by CE. Plants were watered with the indicated NaCl concentrations, and the collected EBC sap showed an increase in all three measured cation species upon salt stress. (Twenty bladders per experiment; $n \geq 6$ experiments, mean \pm SEM). Bars: (a, b) 50 μm ; (c) 25 μm .

sucrose (Sivitz *et al.*, 2007; Gora *et al.*, 2012; Reinders *et al.*, 2012). To illustrate the sugar shuttle through SCs, we used the fluorescent β -glucoside esculin to trace leaf–stalk–bladder sucrose transport. Quinoa leaves were fed via the petiole, and leaf disks were incubated for 1 h in a 1 mM esculin solution. By monitoring the esculin fluorescence in SCs, transcellular shuttle through these cells could be observed (Fig. 2b). Upon closer examination, the sucrose substitute travels all along the EC though the SC, finally appearing in the EBC cytoplasm (Fig. 2c).

Given that EBCs act as a sequestration organ under salinity and that all ions found in the EBC must pass through the SC, we analysed the major cation quantity of the sap found in the bladder using capillary electrophoresis. Under salt stress conditions, the collected EBC sap not only contained increased Na^+ ion quantities, but also increases in K^+ (Fig. 2d,e). Interestingly, besides the two major cations, Na^+ and K^+ , the capillary electrophoresis data also revealed an increase in the nitrogen source ammonium (NH_4^+) in EBCs when plants were subjected to salt stress (Fig. 2d,e).

To track ions released across the SC apical membrane, we used ion-selective MIFE-microelectrodes (Fig. 3b) (Shabala *et al.*, 2006) to measure the ion fluxes through the SCs in leaves under salinity stress. In plants exposed to 200 mM NaCl, we could detect significant effluxes from SCs for all previously analysed cations (Na^+ , K^+ , NH_4^+ ; Table 1 and Fig. 4a–c). Also, for Cl^- , the prominent anion under NaCl-stress, an average efflux rate of $5249 \text{ nmol m}^{-2} \text{ s}^{-1}$ was recorded (Table 1; Fig. 4d). Compared to control plants, exposure to NaCl significantly increased all net ion (Na^+ , K^+ , NH_4^+ and Cl^-) efflux rates from the SCs 3- to 7-

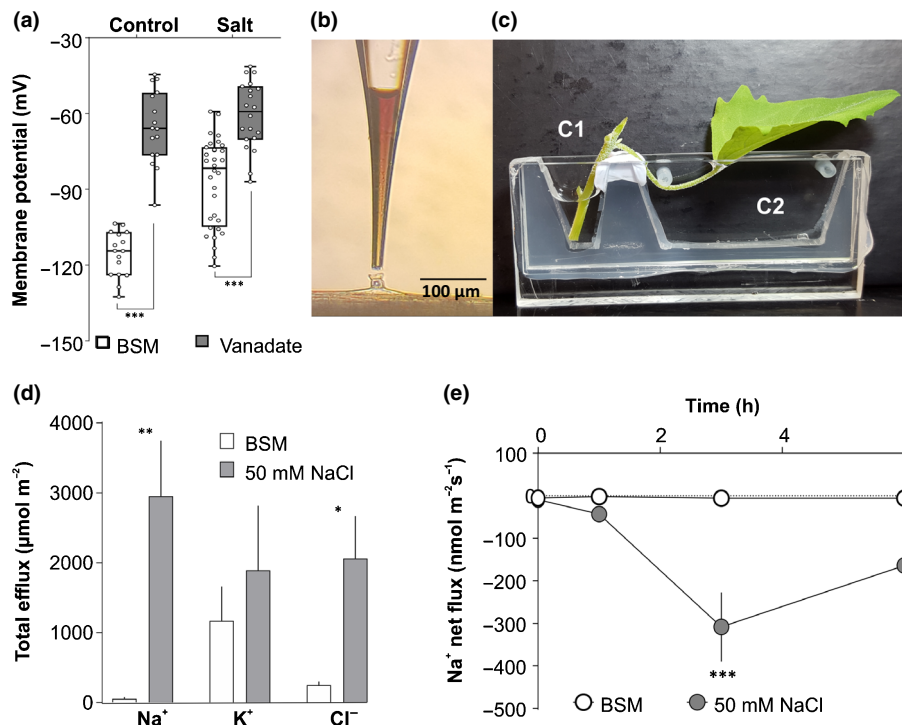


Fig. 3 Salt load in the xylem leads to increases in transcellular ion transport. (a) Membrane potentials measured in stalk cells isolated from *Chenopodium quinoa* plants grown under control or saline (200 mM NaCl) conditions for 5 wk. Stalk cells were isolated by brushing the petioles in a basal salt media (BSM) or in BSM with 0.5 mM sodium orthovanadate. In the box and whisker plots, each point is the value measured on separate stalk cells, depending on the number of stalk cells found in each petiole, and measured on five different petioles from separate plants. The box and whisker plots denote the minimum, 25th percentile, median, 75th percentile and maximum values. (b) Example of a stalk cell and the ion-selective electrode used for the microelectrode ion flux estimation (MIFE) measurements. Bar, 50 μm . (c) Side view of the two-compartment chamber used to monitor the stalk cell transcellular ion transport dynamics with ion-selective microelectrodes following an increase in the salt load of the xylem. Ion fluxes from an isolated stalk cell were measured prior to the addition of 50 mM NaCl in compartment C1 and then measured after 0, 1, 3, and 6 h in the apical pole of a de-bladdered stalk cell in C2. (d) Total sodium (Na^+), potassium (K^+), and chloride (Cl^-) fluxes (as indicated) over 6 h were measured under control conditions (white) and after application of 50 mM NaCl into compartment C1 (grey) ($n = 5$ experiments, mean \pm SEM). (e) Net Na^+ flux during the experiment under control conditions (white circles) and NaCl application (grey circles) ($n = 5$ experiments, mean \pm SEM). Significant differences were calculated using the two-sided Student's t -test (*, $P < 0.05$; **, $P < 0.08$; ***, $P < 0.01$). (See also Supporting Information Fig. S9.)

fold (Table 1; Fig. 4a–d). In addition, we measured a steady-state membrane potential in SCs of -107 mV in control plants and -80 mV in saline grown plants (Fig. 4e).

As leaf bladder density has been shown to decline with leaf age (Fig. S9a), we monitored and compared ion fluxes in young expanding leaves (ELs) and fully expanded leaves (FELs) in plants grown in 200 mM NaCl. In parallel with a decline in bladder density, net Cl^- and Na^+ efflux rates from the SCs declined 4-fold in FELs compared with ELs (Fig. S9b–f).

To monitor the SC transcellular ion transport dynamics, we built a two-compartment recording chamber (Fig. 3c). In this system, a stem segment with a leaf branching off was placed in such a way that the stem segment and base of the petiole were placed in compartment C1, with the upper petiole segment in compartment C2. The lower part of the stem segment in C1 and petiole in C2 were submerged and exposed to BSM. Using this setup, we mimicked a salt-loaded xylem by applying 50 mM NaCl to C1. With ion selective electrodes, we monitored short-term changes in the Na^+ , K^+ , and Cl^- flux rates from the apical pole of a de-bladdered SC in C2 under saline conditions (Fig. 3d). When the petiole was exposed to low saline media, we

Table 1 Stalk cells mediate transcellular cation and anion fluxes.

Ion species	Control treatment net flux ($\text{nmol m}^{-2} \text{s}^{-1}$)	Salt treatment net flux ($\text{nmol m}^{-2} \text{s}^{-1}$)
Sodium	-32 ± 8	-234 ± 39
Potassium	-455 ± 75	-1239 ± 203
Ammonium	-505 ± 79	-2943 ± 335
Chloride	-1183 ± 230	-5249 ± 712

Summary table of net fluxes measured at the apical poles of de-bladdered quinoa (*Chenopodium quinoa*) stalk cells under control and saline (200 mM NaCl) conditions (mean \pm SE). (See also Fig. 4.)

did record marked Na^+ fluxes, with the highest amplitude being observed 3 h after salt application (Fig. 3e), resulting in pronounced Na^+ and Cl^- efflux from the SCs over the 6 h measurement period (Fig. 3d). By contrast, a constant K^+ efflux from SCs was observed in unstressed plants, and this was not affected by the addition of NaCl (Figs 3d, S9g). A significant induction of the K^+ efflux only appeared when the potassium salt instead of NaCl was fed to the petiole (Fig. S9g). The observed flux dynamics illustrate the sequestration of toxic ion concentrations into

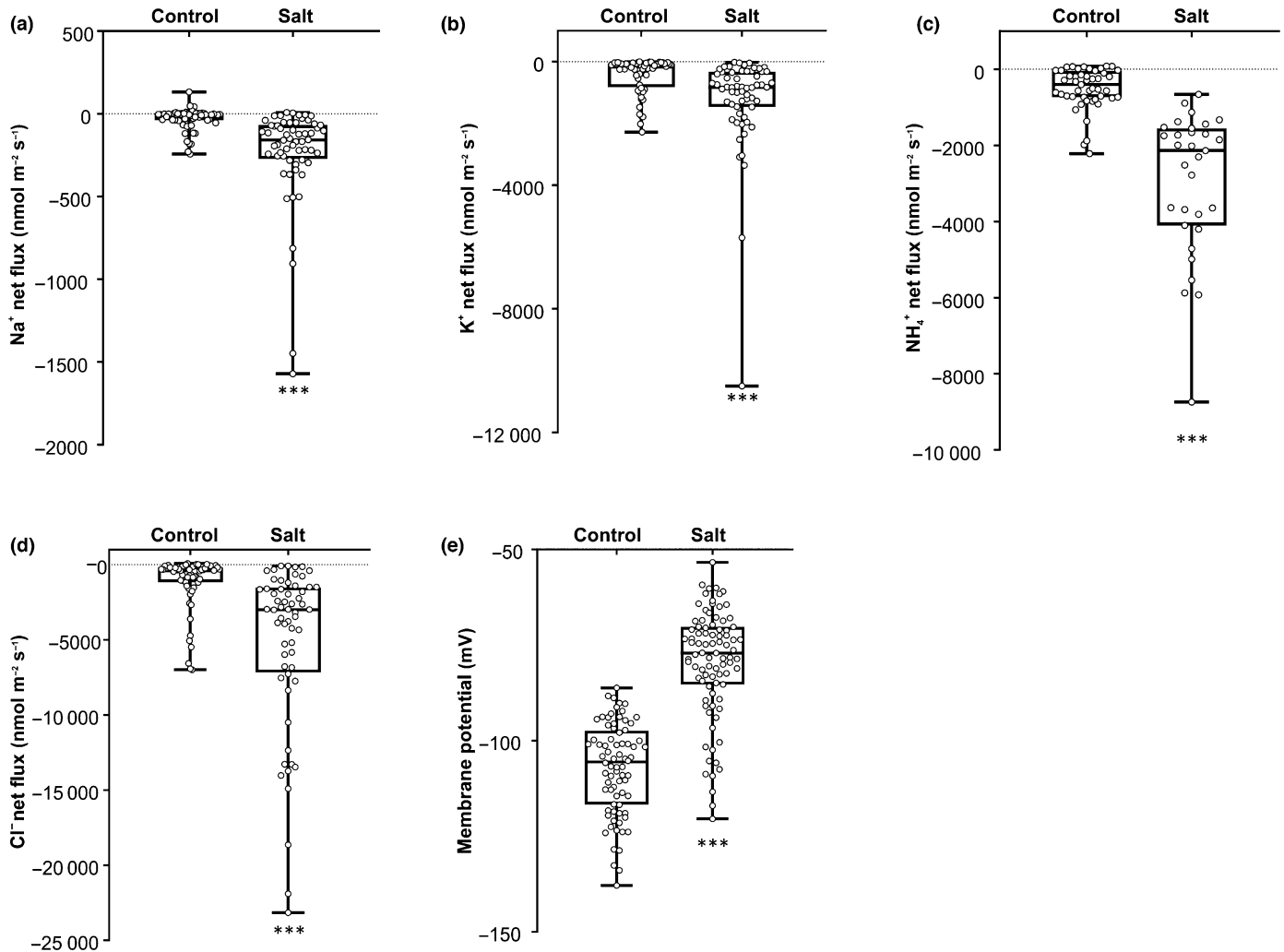


Fig. 4 Salinity enhances ion transport activity in stalk cells. The plots summarise net sodium (Na^+) (a), potassium (K^+) (b), ammonium (NH_4^+) (c), and chloride (Cl^-) (d) fluxes and *Chenopodium quinoa* membrane potentials (e) measured at the apical poles of de-bladdered stalk cells under control and saline (200 mM NaCl) conditions. Each point is the value measured on separate stalk cells, and the box and whisker plots denote the minimum, 25th percentile, median, 75th percentile and maximum values. Significant differences were calculated using the two-sided Student's *t*-test (***, $P < 0.01$). Mean values of ion fluxes can be found in Table 1 and membrane potentials were -107 and -80 mV in control and saline plants, respectively.

EBCs. Overall, these flux experiments along with the capillary electrophoresis measurements provided strong supporting evidence that Na^+ transport within the SC–EBC complex is ultimately coupled to that of K^+ .

The functional expression of stalk cell solute transporters in the *Xenopus* system

Our next step was to investigate the nature of the transporters giving rise to the SC polar ion transport detected in the *in vivo* MIFE experiments shown in Figs 3, 4, and S9. To set up the SC transport model, we searched our RNA-seq data for suitable candidates – well-established in model transport systems processes – whose expression was higher in the SCs (Table S1t). This was the case for SWEET, MFS, AKT1, AMT, and NHX2 type

transporters. To further develop the model, we considered the fact that many transporters are post-translationally regulated. Therefore, we additionally included transporter genes in the model that can be involved in the transport processes and whose SC expression was confirmed (TPM (transcripts per million) > 0.5) and at least twice as high in lightly brushed compared to hard-brushed samples (Table S1t). Of these candidates, we initially focused on the transfer cell transcripts that encode transporters specific for K^+ and NH_4^+ , after which we addressed those able to shuttle Cl^- and Na^+ (Table S1j–o; Fig. S2b).

K^+ transport We first asked the following question: which transporter classes are responsible for shuttling K^+ salts through stalk cells? To enable a 2.8-fold increase in K^+ in EBCs under salt stress (Fig. 2e), the EBC uses the proton motive force (PMF)-

driven high-affinity CqHAK transporter (Bohm *et al.*, 2018). Besides this CqHAK–kinase-sensor complex, a K_{in}^+ channel of the Shaker type could also play a role in K^+ uptake, as indicated by their expression patterns. One AKT1-like channel is upregulated 5-fold in SCs and one high-affinity transporter of the KUP-family is slightly higher (2.4-fold) in SCs. Together, these K^+ channels/transporters might catalyse K^+ uptake on the basal side of SCs (see schematic in Fig. 6).

For K^+ release at the apical SC side, we suspected a Shaker K_{out} channel (CqSKOR) expressed in SCs. To test whether CqSKOR channels fulfil the typical properties of K_{out} channels (Ache *et al.*, 2000), we expressed CqSKOR in *Xenopus* oocytes and analysed its characteristics by means of two-electrode voltage clamp recordings. By applying depolarising voltages in 1, 10 or 100 mM KCl, CqSKOR-expressing oocytes revealed outward rectifying macroscopic currents (Figs 5a, S10a) with a sigmoidal activation kinetic that accelerated upon reduction in the external K^+ concentration (Fig. 5a, inset). The steady-state currents at +40 mV at different external K^+ concentrations explain a K^+_{ext} dependency of CqSKOR with a current-optimum between 3 and 10 mM KCl (Fig. S10b). As expected from Shaker-type K_{out} channels, changing K^+_{ext} shifts the voltage-dependent activation threshold of CqSKOR with the equilibrium potential for K^+ (Fig. S10a). Furthermore, by analysing the open probability of CqSKOR channels, the half-maximal activation voltage ($V_{1/2}$) is shifted to a more negative potential by reducing the external K^+ concentration in the bath (Fig. 5b). Stalk cells depolarise to *c.* –80 mV under salt stress (Figs 3a, 4e), and CqSKOR channels have an optimal current of 3–10 mM K^+_{ext} . Under these conditions, up to 20% of the channels are in the open state, mediating a constant K^+ efflux (Fig. 5b).

NH_4^+ transport As the HAK5-type K^+ transporter can also conduct NH_4^+ in symport with protons (Scherzer *et al.*, 2015), uptake of NH_4^+ into the EBCs (Fig. 2d,e) could be mediated by the EBC-expressed CqHAK transporter (Bohm *et al.*, 2018). Furthermore, Shaker-type K^+ channels of the K^+_{in} subclade are also permeable for ammonium (Very *et al.*, 1995; Hedrich, 2012; Iosip *et al.*, 2020), which raises the question as to whether the SC expressed Shaker-type channel CqSKOR can also release NH_4^+ into the apoplast at the bladder facing side. To test this assumption, 20 mM NH_4Cl was injected into CqSKOR-expressing oocytes, and the macroscopic currents were detected in 3 mM KCl. Before NH_4^+ injection, typical outward directed currents could be observed. These currents declined when NH_4^+ was present in the cytosol (Fig. S10c,d). Hence, instead of having a permeability for NH_4^+ , it can be speculated that ammonium blocks the K^+ efflux through CqSKOR. Nevertheless, NH_4^+ must be shuttled through the SC to get to the EBCs; the NH_4^+ efflux mediated by the SCs of salt-treated quinoa (200 mM NaCl) plants was 3.6-fold higher than under control conditions (Table 1; Fig. 4c). Thus, we searched for transcript homologs of NH_4^+ transporters that are expressed in SCs and identified CqAMT1, a type I classified NH_4^+ transporter, which is 3.7-times more present in lightly brushed than hard-brushed samples (Pantoja, 2012; Scherzer *et al.*, 2013). We functionally expressed this quinoa NH_4^+ transporter in *Xenopus* oocytes, and it could be

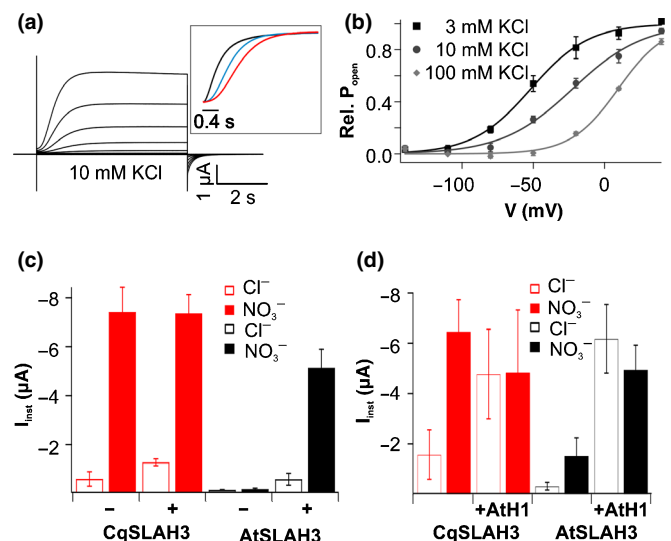


Fig. 5 Functional characterisation of SC-expressed efflux channels. (a) Whole-cell current response of a representative CqSKOR-expressing *Xenopus* oocyte. Outward rectifying currents were elicited in response to depolarising membrane potentials in a bath solution containing 10 mM potassium chloride (KCl) at pH 7.4. The inset plot shows the activation kinetics for 1 mM (black), 10 mM (blue) and 100 mM KCl (red), which accelerate with decreasing external potassium (K^+_{ext}) concentrations. To illustrate the acceleration, the currents at +40 mV and at different K^+ concentrations were normalised from 0 to 1. (b) The relative open probability values for CqSKOR-expressing oocytes at the indicated external K^+ concentrations at pH 7.4 are plotted against the applied voltages. The half-maximal activation potential ($V_{1/2}$) shifted to more negative membrane potentials when KCl was reduced in the bath solution ($n = 4$ experiments, mean \pm SD). (c, d) Instantaneous whole currents (I_{inst}) at –100 mV in oocytes expressing either CqSLAH3 or AtSLAH3 in the presence or absence of (c) AtCPK21delEF or (d) AtSLAH1. Currents were recorded in standard buffers containing either 100 mM chloride or nitrate ($n \geq 4$ experiments, mean \pm SD). (See also Fig. S10.)

localised at the PM when the channel was N-terminally tagged with yellow fluorescent protein (YFP; Fig. S10e, inset). By perfusing CqAMT1-expressing oocytes with 2 mM NH_4Cl , currents of up to –35 nA at –160 mV could be recorded (Fig. S10e).

Cl^- transport For anion-related transport, the most prominent SC genes belong to the ‘MFS superfamily’, which represents the largest group of secondary active membrane transporters. MFS family members have been associated with Cl^- uptake (Nino-Gonzalez *et al.*, 2019), so it is tempting to speculate that SC MFSs are involved in Cl^- uptake at the basal membrane. To gain efficient anion sequestration and accumulation in EBCs to compensate for the electric charge from cation uptake, the respective anions need to be released from SCs into the apoplast for a subsequent uptake into the EBCs. In Arabidopsis, members of the S-type anion channel family were shown to mediate anion efflux from different tissues and cell types (Hedrich & Geiger, 2017). In roots, SLAH3 mediates the efflux of nitrate and Cl^- into the xylem sap for further transport to the shoot (Cubero-Font *et al.*, 2016).

Interestingly, transcripts of a SLAH3-type channel were not differentially expressed between hard-brushed and lightly brushed samples and were depleted 5.3-fold in EBCs. This illustrates the

presence of CqSLAH3 transcripts in SCs and ECs, so it represents a good candidate for the anion release channel in quinoa (Table 1; Fig. 4d).

Accordingly, we expressed CqSLAH3 in oocytes for detailed characterisation of channel features. Previous studies showed that AtSLAH3 is electrically silent when expressed alone in the oocyte system, but the channel can be activated either via phosphorylation by kinases (Meyerhoff *et al.*, 2005; Geiger *et al.*, 2011; Liu *et al.*, 2019) or via direct interaction with the silent S-type anion channel subunit SLAH1 (Cubero-Font *et al.*, 2016) (Fig. 5c,d). By contrast, quinoa SLAH3 was found to be constitutively active when expressed alone in oocytes (Fig. 5c), reminiscent of PttSLAH3, which is involved in the secretion of anions from poplar extrafloral nectaries (Jaborsky *et al.*, 2016). Furthermore, current amplitude in a nitrate-based solution was independent of the presence of the Arabidopsis kinase CPK21 or the channel subunit AtSLAH1 (Fig. 5c,d). In line with a known characteristic for SLAH3-type channels (Geiger *et al.*, 2011), the presence of extracellular nitrate was a prerequisite for CqSLAH3 activity (Fig. S10f). Nonetheless, although CqSLAH3 shows a strong preference for nitrate over Cl^- (Fig. S10g), detailed analysis revealed that the channel is permeable for Cl^- in the presence of nitrate, as indicated by a shift in the reversal potential to more negative membrane potentials with an increasing external Cl^- concentration (Fig. S10h). This Cl^- conductance can be strongly increased by co-expression with AtSLAH1 (Fig. 5d), implying that modulation of CqSLAH3 characteristics via SLAH1 could drive Cl^- efflux. Like CqSLAH3, transcripts of the quinoa ortholog to AtSLAH1 could be found in SCs and ECs, underlying the role of CqSLAH3 in Cl^- release from SCs.

Na^+ transport Because EBCs function as a dump for toxic sodium under salt stress (Shabala *et al.*, 2014; Kiani-Pouya *et al.*, 2017; Bohm *et al.*, 2018), we addressed the ability to direct Na^+ across the SCs into these cells. The electroneutral SOS1-type system that pushes Na^+ out of the cell in exchange for H^+ is expressed in SCs (Table S1k). The same SC expression pattern was observed for the Na^+ inward rectifier CqHKT1.2, which also functions in EBCs (Bohm *et al.*, 2018). Thus, CqHKT1.2 mediates a one-way Na^+ route through the SC into the EBC. The expression profile of SCs (Table S1; Fig. S2b) suggests that the amount of Na^+ transferred to the EBCs via the SCs is regulated by transporter activity rather than transcript quantity. This is in line with the observation of little regulation by transcriptional changes in Na^+ transport processes in salt stressed EBCs. Therefore, it can be assumed that SCs have a similar constituent activity of Na^+ sequestration to that of EBCs (Bohm *et al.*, 2018), transferring Na^+ and Cl^- according to salt stress associated demands.

Discussion

Ultrastructure and gene expression meet transfer cell function

The SC transcriptome mirrors the function of a transfer cell, which based on TEM tomography, can be subdivided into two

major zones (upper and lower sides). Given that root hairs are also polarised structures, we were not surprised to find genes expressed in polarised SCs that are related to those in root hairs. We found strong evidence that SCs are metabolically very active: first, the apical part consists of numerous mitochondria; second, most of the organelles are embedded in a dense cytoplasm; and third, the nuclear euchromatin appears open. In line with a cell involved in highly energy-dependent solute transport activity, SCs are enriched in ATP generating mitochondria, and ABC transporters are strongly upregulated. The presence of PDs in the scanning electron microscope images suggests a symplastic pathway into the stalk cell. However, the staining experiments show that this pathway is not open all the way into the EBC. We hypothesise that the permeability of the PDs is regulated during bladder evolution. When bladders mature and gain turgor, PDs on the apical side of the SC may close. This notion of switchable PDs is supported by SC expression of regulatory PDLP genes. Ions, sugars and metabolites arriving in the epidermis enter the SC and exit this transfer cell into the EBC through transmembrane channels, pumps and carriers. Based on this polar scenario plus the transporter genes expressed and electrophysiologically analysed *in vivo* and in *Xenopus* oocytes, we examined how SCs mediate transcellular cation and anion fluxes along with those responsible for sugar and metabolite transfer (Fig. 6).

Macronutrients taken up from the soil along with metabolites produced in the leaf are fed into ECs. As such, the chloroplast-deprived ECs represent sinks for ions, sugars, and nitrogen-, phosphorus- and sulphur-rich nutrients. The basal SC membrane must harbour active transport mechanisms to accumulate particular solutes against their concentration gradient. In SCs, proton-coupled symporters such as the MFS, HAKs, and SUCs use both the inward H^+ gradient and membrane potential to drive Cl^- , K^+ and sucrose energetically uphill. The proton driving force is generated by the ATP consuming AHA-type H^+ -ATPase. The potassium ion, like Na^+ and NH_4^+ , is positively charged, and upon membrane hyperpolarisation, these cations traverse AKT, HKT and AMT channels, powered by the electrical force (Fig. 6, left). In addition to these, nonspecific cation channels (Table S1k–m) can also contribute.

The same thermodynamic consideration can be applied to the apical SC membrane. Sucrose, accumulated in SCs by the activity of SUC2 at the basal pole, can use SWEET-type effluxers and the outward directed sugar gradient to exit the cell at the apical pole.

Microelectrode ion flux estimation measurements on SCs recorded a massive Cl^- efflux, most likely mediated by the quinoa orthologs of the high-capacity SLAH3/1 anion channels. When anion channels open, the membrane potential drops, and depolarisation-activated K^+ release channels of the plant Shaker SKOR-type come into play. Outward rectifying SKOR channels transport K^+ , but SKOR has little, if any, affinity for Na^+ . However, the proton-driven Na^+/H^+ SOS1 shuttles Na^+ out of the cell in exchange for H^+ . Upon depolarisation, the AHA-type H^+ -pumps become activated, retaining the pH gradient required for SOS1 Na^+/H^+ transport (Fig. 6, right-hand side).

In plants, sodium stress is known to increase the cytosolic calcium concentration (Knight *et al.*, 1997), resulting in a greater

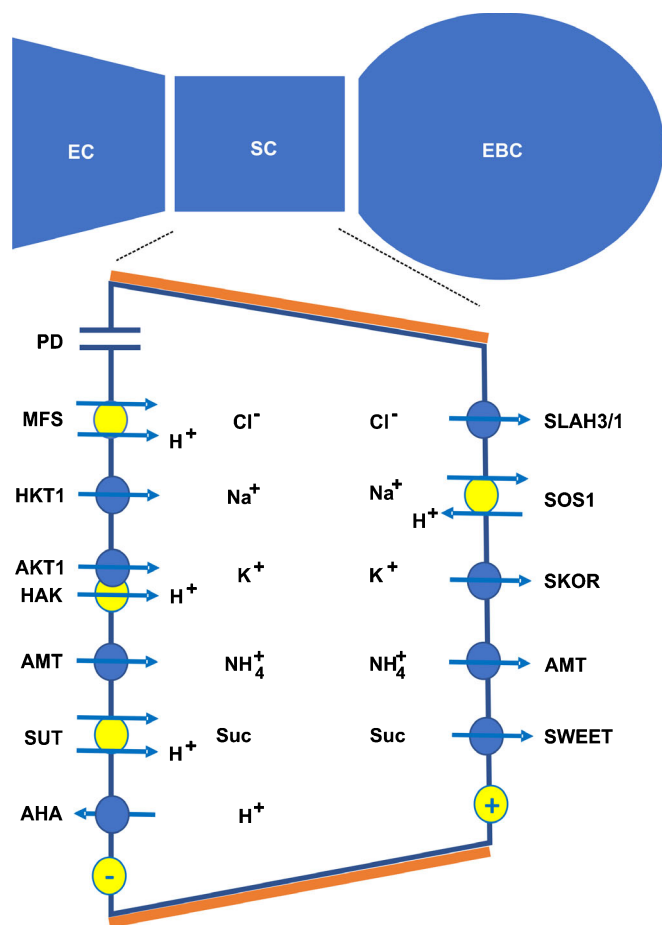


Fig. 6 Working model of stalk cell shuttle systems. The upper section illustrates the *Chenopodium quinoa* epidermal-cell–stalk-cell–bladder-cell (EC–SC–EBC) complex. A stalk cell is schematically magnified in the lower part, and the underlying transport systems for ion and sugar transfer into bladder cells are indicated, including plasmodesmata (PD). An electrical gradient (lower circles) within the SC is likely due to the polarised distribution of transport proteins and/or ions. The involvement of the proton motive force in symport and/or antiport processes is marked in yellow. Stalk cells have lateral thick lateral cell walls and cuticles (orange) for stability purposes as well as to prevent ion leakage and to electrically isolate the SCs.

tolerance of salt loads. This tolerance involves the SOS pathway, which is regulated in a Ca^{2+} -dependent manner and consists of the Ca^{2+} sensor SOS3, the protein kinase SOS2 and the Na^+/H^+ antiporter SOS1. However, the nature of the transporter controlling salt-induced Ca^{2+} -influx has not yet been identified (Hedrich, 2012; Zhu, 2016). Recently MOCA1, a glucuronosyltransferase for GIPC-sphingolipids in the PM, was identified as a molecular component essential for salinity-induced calcium elevation, depolarisation, and Na^+/H^+ antiporter activation (Jiang *et al.*, 2019; Kahlenberg *et al.*, 2020). Notably, an ortholog of MOCA1 is found in quinoa (Table S1p). Consistent with its important role in the salt-induced calcium signalling pathway, the glucuronosyltransferase was found with median TPM values of 7.75, 7.85 and 11.85 in the SC enriched fraction. This underscores the hypotheses that salinity induced transport

processes are subject to a regulatory component rather than an induced expression of the transport proteins themselves, and that one regulatory component could be Ca^{2+} ions, which modulate the sodium sensing and transport machinery (Fig. S2b). Interestingly, we also found a gene annotated for ‘GLR ligand-gated cation channel’ that was upregulated 384 times (Table S1b). GLRs in plants have been associated with calcium waves and signalling, and represent the Ca^{2+} entry pathway critical for electrical signals (Meyerhoff *et al.*, 2005; Nguyen *et al.*, 2018; Toyota *et al.*, 2018). Future studies will show whether the SC GLR gene can rescue mutants hypersensitive to salt and/or impaired in Ca^{2+} signalling.

Although the genomic information of quinoa is available (Yasui *et al.*, 2016; Jarvis *et al.*, 2017; Zou *et al.*, 2017), the lack of analysis of the gene function *in planta* was still a limiting factor. The findings reported in this study fill this void and may be a potential game-changer in developing crop species with the ability to secrete/store excessive salt loads in their trichomes. This represents a previously untapped resource for regaining the salt tolerance present in wild relatives of modern crops that was lost during their domestication (López-Marqués *et al.*, 2020). While, to the best of our knowledge, protocols for applying CRISPR techniques to quinoa species have not been developed yet, Ogata *et al.* (2021) have recently demonstrated that virus-mediated expression and gene silencing can be used in quinoa plants. This tool will provide more detailed insight into the salt stress physiology of quinoa in future research and presents an opportunity to test previously established working models. Once the function of key genes is demonstrated *in planta*, trichome-specific promoters may be used to introgress them into crop quinoa relatives, thereby improving their salinity tolerance and minimising salinity-induced crop losses.

Acknowledgements

We wish to thank Daniela Bunsen (University of Würzburg) for her assistance in preparing the samples for the 3D-EM. This work was supported by the DFG (Deutsche Forschungsgemeinschaft) grant SCHE 2148/1-1 to S Scherzer and grant HE 1640/44-1 to RH, the DFG – INST 93/1003-1 FUGG (426173797), the Strategic Priority Research Program of CAS (XDB27040108 to HZ and XDB27040101 to J-KZ), the King Saud University’s International Cooperation and Scientific Twinning Dept., Riyadh, Saudi Arabia (Project ICSTD-2020/2), the King Saud University’s Distinguished Fellowship Program, Riyadh, Saudi Arabia to KFXM, the Australian Research Council (DP150101663), National Distinguished Expert Project (WQ20174400441), and grant no. 31961143001 for Joint Research Projects between the Pakistan Science Foundation and the National Natural Science Foundation China to S Shabala. NB was a recipient of the Marie Curie Fellowship funded by the EU (grant no. 700001).

Competing interests

The authors declare no competing interests.

Author contributions

KFXM, S Shabala, KASA-R, SH, SA, SM, J-KZ, RH and S Scherzer designed the research; NB, JB, MM, CS, HMM, TM, JC, CF, SH, HZ and S Scherzer performed the research; NB, JB, SH, MB, PA and S Scherzer analysed data; CS and CF performed the ultrastructural analysis of stalk cells; MM and KFXM performed the bioinformatic analysis; NB, JB, MM, TAC, S Shabala, J-KZ, RH and S Scherzer wrote the paper. NB, JB and MM contributed equally to this work.

ORCID

Peter Ache  <https://orcid.org/0000-0002-2902-7552>
 Khaled A. S. Al-Rasheid  <https://orcid.org/0000-0002-3404-3397>
 Saleh Alquraishi  <https://orcid.org/0000-0002-9629-7288>
 Jennifer Böhm  <https://orcid.org/0000-0002-8104-8705>
 Nadia Bazihizina  <https://orcid.org/0000-0003-4856-0659>
 Michael Breadmore  <https://orcid.org/0000-0001-5591-4326>
 Joan Cabot  <https://orcid.org/0000-0002-3305-078X>
 Tracey Ann Cuin  <https://orcid.org/0000-0002-7026-1500>
 Christian Fella  <https://orcid.org/0000-0002-5932-9295>
 Rainer Hedrich  <https://orcid.org/0000-0003-3224-1362>
 Shouguang Huang  <https://orcid.org/0000-0001-7007-0301>
 Heike M. Müller  <https://orcid.org/0000-0002-9316-6493>
 Tobias Maierhofer  <https://orcid.org/0000-0002-6839-4240>
 Stefano Mancuso  <https://orcid.org/0000-0003-1752-3986>
 Klaus F. X. Mayer  <https://orcid.org/0000-0001-6484-1077>
 Maxim Messerer  <https://orcid.org/0000-0003-0554-5045>
 Sönke Scherzer  <https://orcid.org/0000-0002-7197-2101>
 Sergey Shabala  <https://orcid.org/0000-0003-2345-8981>
 Christian Stigloher  <https://orcid.org/0000-0001-6941-2669>
 Heng Zhang  <https://orcid.org/0000-0002-1541-3890>
 Jian-Kang Zhu  <https://orcid.org/0000-0001-5134-731X>

Data availability

RNA-seq data have been deposited in the ArrayExpress database at EMBL-EBI (<http://www.ebi.ac.uk/arrayexpress>). Stalk cell study: Array Express ID: E-MTAB-10363; quinoa ABA study: Array Express ID: E-MTAB-10419. Quinoa transport proteins: CqSKOR (TRINITY_GG_83_c4_g1), CqSLAH3 (TRINITY_GG_29628_c18_g1), CqAMT (TRINITY_GG_1769_c6_g1).

References

- Ache P, Becker D, Ivashikina N, Dietrich P, Roelfsema MR, Hedrich R. 2000. GORK, a delayed outward rectifier expressed in guard cells of *Arabidopsis thaliana*, is a K⁺-selective, K⁺-sensing ion channel. *FEBS Letters* 486: 93–98.
- Bohm J, Messerer M, Muller HM, Scholz-Starke J, Gradogna A, Scherzer S, Maierhofer T, Bazihizina N, Zhang H *et al.* 2018. Understanding the molecular basis of salt sequestration in epidermal bladder cells of *Chenopodium quinoa*. *Current Biology* 28: 3075–3085.
- Cilia ML, Jackson D. 2004. Plasmodesmata form and function. *Current Opinion in Cell Biology* 16: 500–506.
- Cubero-Font P, Maierhofer T, Jaslan J, Rosales M, Espartero J, Díaz-Rueda P, Müller H, Hürter A-L, Al-Rasheid K, Marten I *et al.* 2016. Silent S-type anion channel subunit SLAH1 gates SLAH3 open for chloride root-to-shoot translocation. *Current Biology* 26: 2213–2220.
- Deeken R, Ache P, Kajahn I, Klinkenberg J, Bringmann G, Hedrich R. 2008. Identification of *Arabidopsis thaliana* phloem RNAs provides a search criterion for phloem-based transcripts hidden in complex datasets of microarray experiments. *The Plant Journal* 55: 746–759.
- Dindas J, Scherzer S, Roelfsema MRG, von Meyer K, Muller HM, Al-Rasheid KAS, Palme K, Dietrich P, Becker D *et al.* 2018. AUX1-mediated root hair auxin influx governs SCF(TIR1/AFB)-type Ca²⁺ signaling. *Nature Communications* 9: 1174.
- Flowers TJ, Colmer TD. 2008. Salinity tolerance in halophytes. *New Phytologist* 179: 945–963.
- Geiger D, Maierhofer T, Al-Rasheid KA, Scherzer S, Mumm P, Liese A, Ache P, Wellmann C, Marten I *et al.* 2011. Stomatal closure by fast abscisic acid signaling is mediated by the guard cell anion channel SLAH3 and the receptor RCAR1. *Science Signalling* 4: ra32.
- Gora PJ, Reinders A, Ward JM. 2012. A novel fluorescent assay for sucrose transporters. *Plant Methods* 8: 13.
- Hariadi Y, Marandon K, Tian Y, Jacobsen SE, Shabala S. 2011. Ionic and osmotic relations in quinoa (*Chenopodium quinoa* Willd.) plants grown at various salinity levels. *Journal of Experimental Botany* 62: 185–193.
- Hedrich R. 2012. Ion channels in plants. *Physiological Reviews* 92: 1777–1811.
- Hedrich R, Geiger D. 2017. Biology of SLAC1-type anion channels - from nutrient uptake to stomatal closure. *New Phytologist* 216: 46–61.
- Iosip AL, Bohm J, Scherzer S, Al-Rasheid KAS, Dreyer I, Schultz J, Becker D, Kreuzer I, Hedrich R. 2020. The venus flytrap trigger hair-specific potassium channel KDM1 can reestablish the K⁺ gradient required for hapto-electric signaling. *PLoS Biology* 18: e3000964.
- Ivashikina N, Deeken R, Ache P, Kranz E, Pommerrenig B, Sauer N, Hedrich R. 2003. Isolation of AtSUC2 promoter-GFP-marked companion cells for patch-clamp studies and expression profiling. *The Plant Journal* 36: 931–945.
- Jaborsky M, Maierhofer T, Olbrich A, Escalante-Perez M, Muller HM, Simon J, Krol E, Cuin TA, Fromm J *et al.* 2016. SLAH3-type anion channel expressed in poplar secretory epithelia operates in calcium kinase CPK-autonomous manner. *New Phytologist* 210: 922–933.
- Jakoby MJ, Falkenhan D, Mader MT, Brininstool G, Wischnitzki E, Platz N, Hudson A, Hulskamp M, Larkin J *et al.* 2008. Transcriptional profiling of mature *Arabidopsis* trichomes reveals that NOECK encodes the MIXTA-like transcriptional regulator MYB106. *Plant Physiology* 148: 1583–1602.
- Jarvis DE, Ho YS, Lightfoot DJ, Schmöckel SM, Li BO, Borm TJA, Ohyanagi H, Mineta K, Michell CT, Saber N *et al.* 2017. The genome of *Chenopodium quinoa*. *Nature* 542: 307–312.
- Jiang Z, Zhou X, Tao M, Yuan F, Liu L, Wu F, Wu X, Xiang Y, Niu Y, Liu F *et al.* 2019. Plant cell-surface GIPC sphingolipids sense salt to trigger Ca²⁺ influx. *Nature* 572: 341–346.
- Kahlenberg CA, Nwachukwu BU, Mehta N, Zhang DT, Nguyen J, Fabricant PD, Altchek DW, Williams RJ, Allen AA. 2020. Development and validation of the hospital for special surgery anterior cruciate ligament postoperative satisfaction survey. *Arthroscopy* 36: 1897–1903.
- Karremans MA, Ruthensteiner B, Mercier L, Schieber NL, Solecki G, Winkler F, Goetz JG, Schwab Y. 2017. Find your way with X-Ray: using microCT to correlate *in vivo* imaging with 3D electron microscopy. *Methods in Cell Biology* 140: 277–301.
- Kiani-Pouya A, Roessner U, Jayasinghe NS, Lutz A, Rupasinghe T, Bazihizina N, Bohm J, Alharbi S, Hedrich R, Shabala S. 2017. Epidermal bladder cells confer salinity stress tolerance in the halophyte quinoa and *Atriplex* species. *Plant, Cell & Environment* 40: 1900–1915.
- Kim JM, Sasaki T, Ueda M, Sako K, Seki M. 2015. Chromatin changes in response to drought, salinity, heat, and cold stresses in plants. *Frontiers in Plant Science* 6: 114.
- Knight H, Trethewey AJ, Knight MR. 1997. Calcium signalling in *Arabidopsis thaliana* responding to drought and salinity. *The Plant Journal* 12: 1067–1078.
- Koyro HW, Eisa SS. 2008. Effect of salinity on composition, viability and germination of seeds of *Chenopodium quinoa* Willd. *Plant and Soil* 302: 79–90.

- Kremer JR, Mastrorade DN, McIntosh JR. 1996. Computer visualization of three-dimensional image data using IMOD. *Journal of Structural Biology* 116: 71–76.
- Liu N-J, Zhang T, Liu Z-H, Chen X, Guo H-S, Ju B-H, Zhang Y-Y, Li G-Z, Zhou Q-H, Qin Y-M *et al.* 2020. Phytosphinganine affects plasmodesmata permeability via facilitating PDLP5-stimulated callose accumulation in arabidopsis. *Molecular Plant* 13: 128–143.
- Liu Y, Maierhofer T, Rybak K, Sklenar J, Breakspear A, Johnston MG, Fliegmann J, Huang S, Roelfsema MRG *et al.* 2019. Anion channel SLAH3 is a regulatory target of chitin receptor-associated kinase PBL27 in microbial stomatal closure. *eLife* 8: e44474.
- López-Marqués RL, Nørrevang AF, Ache P, Moog M, Visintainer D, Wendt T, Østerberg JT, Dockter C, Jørgensen ME, Salvador AT *et al.* 2020. Prospects for the accelerated improvement of the resilient crop quinoa. *Journal of Experimental Botany* 71: 5333–5347.
- Meyerhoff O, Müller K, Roelfsema MRG, Latz A, Lacombe B, Hedrich R, Dietrich P, Becker D. 2005. AtGLR3.4, a glutamate receptor channel-like gene is sensitive to touch and cold. *Planta* 222: 418–427.
- Nakamura M, Grebe M. 2018. Outer, inner and planar polarity in the Arabidopsis root. *Current Opinion in Plant Biology* 41: 46–53.
- Nguyen CT, Kurenda A, Stolz S, Chételat A, Farmer EE. 2018. Identification of cell populations necessary for leaf-to-leaf electrical signaling in a wounded plant. *Proceedings of the National Academy of Sciences, USA* 115: 10178–10183.
- Nino-Gonzalez M, Novo-Uzal E, Richardson DN, Barros PM, Duque P. 2019. More transporters, more substrates: the arabidopsis major facilitator superfamily revisited. *Molecular Plant* 12: 1182–1202.
- Ogata T, Toyoshima M, Yamamizo-Oda C, Kobayashi Y, Fujii K, Tanaka K, Tanaka T, Mizukoshi H, Yasui Y *et al.* 2021. Virus-mediated transient expression techniques enable functional genomics studies and modulations of betalain biosynthesis and plant height in quinoa. *Frontiers in Plant Science* 12: 643499.
- Pantoja O. 2012. High affinity ammonium transporters: molecular mechanism of action. *Frontiers in Plant Science* 3: 34.
- Park K, Knoblauch J, Oparka K, Jensen KH. 2019. Controlling intercellular flow through mechanosensitive plasmodesmata nanopores. *Nature Communications* 10: 3564.
- Probst AV, Mittelsten SO. 2015. Stress-induced structural changes in plant chromatin. *Current Opinion in Plant Biology* 27: 8–16.
- Pu J, Cao L, McCaig CD. 2015. Physiological extracellular electrical signals guide and orient the polarity of gut epithelial cells. *Tissue Barriers* 3: e1037417.
- Reinders A, Sivitz AB, Ward JM. 2012. Evolution of plant sucrose uptake transporters. *Frontiers in Plant Science* 3: 22.
- Reisen D, Marty F, Leborgne-Castel N. 2005. New insights into the tonoplast architecture of plant vacuoles and vacuolar dynamics during osmotic stress. *BMC Plant Biology* 5: 13.
- Ruiz-Sola MÁ, Arbona V, Gómez-Cadenas A, Rodríguez-Concepción M, Rodríguez-Villalón A. 2014. A root specific induction of carotenoid biosynthesis contributes to ABA production upon salt stress in Arabidopsis. *PLoS ONE* 9: e90765.
- Scherzer S, Böhm J, Krol E, Shabala L, Kreuzer I, Larisch C, Bemm F, Al-Rasheid KAS, Shabala S, Rennenberg H *et al.* 2015. Calcium sensor kinase activates potassium uptake systems in gland cells of Venus flytraps. *Proceedings of the National Academy of Sciences, USA* 112: 7309–7314.
- Scherzer S, Krol E, Kreuzer I, Kruse J, Karl F, von Rüden M, Escalante-Perez M, Müller T, Rennenberg H, Al-Rasheid K *et al.* 2013. The *Dionaea muscipula* ammonium channel DmAMT1 provides NH₄⁺ uptake associated with Venus flytrap's prey digestion. *Current Biology* 23: 1649–1657.
- Scherzer S, Shabala L, Hedrich B, Fromm J, Bauer H, Munz E, Jakob P, Al-Rasheid KAS, Kreuzer I, Becker D *et al.* 2017. Insect haptoelectrical stimulation of Venus flytrap triggers exocytosis in gland cells. *Proceedings of the National Academy of Sciences, USA* 114: 4822–4827.
- Shabala L, Ross T, McMeekin T, Shabala S. 2006. Non-invasive microelectrode ion flux measurements to study adaptive responses of microorganisms to the environment. *FEMS Microbiology Reviews* 30: 472–486.
- Shabala S, Bose J, Hedrich R. 2014. Salt bladders: do they matter? *Trends in Plant Science* 19: 687–691.
- Sivitz AB, Reinders A, Johnson ME, Krentz AD, Grof CP, Perroux JM, Ward JM. 2007. Arabidopsis sucrose transporter AtSUC9. High-affinity transport activity, intragenic control of expression, and early flowering mutant phenotype. *Plant Physiology* 143: 188–198.
- Thimm O, Bläsing O, Gibon Y, Nagel A, Meyer S, Krüger P, Selbig J, Müller LA, Rhee SY, Stitt M. 2004. MapMan: a user-driven tool to display genomics data sets onto diagrams of metabolic pathways and other biological processes. *The Plant Journal* 37: 914–939.
- Toyota M, Spencer D, Sawai-Toyota S, Jiaqi W, Zhang T, Koo AJ, Howe GA, Gilroy S. 2018. Glutamate triggers long-distance, calcium-based plant defense signaling. *Science* 361: 1112–1115.
- Tucker EB. 1990. Calcium-loaded 1,2-bis(2-aminophenoxy)ethane-*N, N, N', N'*-tetraacetic acid blocks cell-to-cell diffusion of carboxyfluorescein in staminal hairs of *Setcreasea purpurea*. *Planta* 182: 34–38.
- Very AA, Gaymard F, Bosseux C, Sentenac H, Thibaud JB. 1995. Expression of a cloned plant K⁺ channel in *Xenopus* oocytes: analysis of macroscopic currents. *The Plant Journal* 7: 321–332.
- Yang Z. 2008. Cell polarity signaling in Arabidopsis. *Annual Review of Cell and Developmental Biology* 24: 551–575.
- Yasui Y, Hirakawa H, Oikawa T, Toyoshima M, Matsuzaki C, Ueno M, Mizuno N, Nagatoshi Y, Imamura T *et al.* 2016. Draft genome sequence of an inbred line of *Chenopodium quinoa*, an allotetraploid crop with great environmental adaptability and outstanding nutritional properties. *DNA Research* 23: 535–546.
- Ye ZW, Chen QF, Chye ML. 2017. Arabidopsis thaliana Acyl-CoA-binding protein ACBP6 interacts with plasmodesmata-located protein PDLP8. *Plant Signaling & Behavior* 12: e1359365.
- You Y, Sawikowska A, Lee JE, Benstein RM, Neumann M, Krajewski P, Schmid M. 2019. Phloem companion cell-specific transcriptomic and epigenomic analyses identify MRF1, a regulator of flowering. *Plant Cell* 31: 325–345.
- Zhu J-K. 2016. Abiotic stress signaling and responses in plants. *Cell* 167: 313–324.
- Zörb C, Geilfus C-M, Dietz K-J. 2019. Salinity and crop yield. *Plant Biology* 21: 31–38.
- Zou C, Chen C, Xiao L, Müller HM, Ache P, Haberer G, Zhang M, Jia W, Deng P *et al.* 2017. A high-quality genome assembly of quinoa provides insights into the molecular basis of salt bladder-based salinity tolerance and the exceptional nutritional value. *Cell Research* 27: 1327–1340.

Supporting Information

Additional Supporting Information may be found online in the Supporting Information section at the end of the article.

Fig. S1 Bioinformatical analysis of stalk cells.

Fig. S2 The number of differentially expressed genes is far higher in stalk cells compared to epidermal bladder cells.

Fig. S3 Ultrastructure of stalk cells.

Fig. S4 Stalk cell isolation procedure and vitality check of the de-bladdered stalk cell for bioinformatical analysis.

Fig. S5 Staining experiments show no symplastic connection between stalk cells and epidermal bladder cells and a trans-stalk cell voltage gradient.

Fig. S6 Gene ontology term ‘biological process’.

Fig. S7 Gene ontology term ‘cellular component’.

Fig. S8 Gene ontology term ‘molecular function’.

Fig. S9 Ion fluxes in stalk cells on petioles of quinoa leaves (accession Q20).

Fig. S10 Electrophysiological characteristics of stalk cell expressed transport proteins.

Method S1 Additional materials and methods.

Table S1 Bioinformatical analysis of the stalk cell transcriptome.

Video S1 Combination of X-ray imaging of a resin embedded sample to efficiently target stalk cell of interest and serial section transmission electron microscopy imaging for analysis of the ultrastructure at high resolution and 3D.

Please note: Wiley Blackwell are not responsible for the content or functionality of any Supporting Information supplied by the authors. Any queries (other than missing material) should be directed to the *New Phytologist* Central Office.